ISSN (Print) : 0974-6846
ISSN (Online) : 0974-5645
Indian Journal of Science and Technology, *Vol 10(28), DOI: 10.17485/ijst/2017/v10i28/115056, July 2017*

Diagnosis of Abdominal Cancer Tumour by Fusion Technique and Treatment using Radio Frequency Heat

Shirish S. Kulkarni[1], Sachin B. Umbarkar[2] , R. N. Awale[1] and Abhay Wagh[3]

[1]Department of Electrical Engineering, Mumbai University, Veermata Jijabai Technological Institute, Mumbai – 400031, Maharashtra, India; shirishkulkarni1966@gmail.com, rnawale@vjti.org.in
[2]Department of Electronics Engineering, Mumbai University, Ramrao Adik Institute of Technology, Mumbai – 400706, Maharashtra, India; sachin.umb@gmail.com
[3]MSBTE, Mumbai – 400051, Maharashtra, India; waghabhay14@gmail.com

Abstract

Objectives: To propose a better image fusion approach for detecting different stages of cancer and suggesting suitable technique for treating cancer to medical practitioners. **Methods:** Diagnosis of cancerous region is carried out by wavelet based fusion technique on PET/CT images and the thermal effect on cancer tissue growth is analysed using RF module of COMSOL-Multi-physics software. **Findings:** Multimodal image fusion technique helps to identify the growth of object which is carried out by wavelet technique. The Computed Tomography (CT) scan helps to determine extent of the cancer, while Positron Emisson Tomography (PET) scan finds areas of cancer spread. There after the results acquired will enhance visual effect and help the medical practitioners to examine the development of tumour. In case of tumour, cell spreads beyond the infected portion of the organ, treatment using chemotheraphy is harmful while, surgery can be fatal, and hence Radio Frequency (RF) heating technique may be a better solution. The important issue in cancer treatment is to bind the area of human body under the RF energy influence, to avoid unwanted radiation or heating effects on healthy human tissue. **Applications:** The results acquired will enhance visual effect and help the medical practitioners to examine development of tumour. Further in this paper, the various graphs of temperature variation, electric field distribution, degree of tissue injured, at various times instant versus cancer region are plotted, also expression for the space Eletromagnetic (EM) wave propagation and its mathematical analysis is carried out.

Keywords: Cancer, COMSOL-Multiphysics, Image Fusion, PET/CT, Radio Frequency (RF), Wavelet Transform (WT)

1. Introduction

Nowadays, increasing number of population is prone to various health related issues caused due to stressful work, culture and unhygienic habits. It includes exposure to radiation, consumption of toxic materials like cigarettes, alcohol or other carcinogenic items. This increase in the number of patients has put more attention towards generation of faster and easier methods for finding abnormality. Such systems will aid doctors in analysing critical test reports and scans. The body space between thorax and pelvis is known as abdomen, constitutes of stomach, small and large intestines, pancreas, liver, and gallbladder. Abdominal cancer can be regarded as uncontrolled growth of abnormal cells anywhere in the abdomen.

Detailed literature survey is carried out for variety of modalities like Computed Tomography (CT), Positron Emission Tomography (PET), Magnetic Resonance Imaging (MRI), Single-Photon Emission Computed Tomography (SPECT) and many more that can be combined by fusion techniques, can result in better detection of cancer region.

Particularly in this paper, we have focused on image fusion using PET/CT images for detection of abdo-

**Author for correspondence*

men cancer[1]. Bi-orthogonal transform, with absolute maximum selection and energy based fusion rules for qualitative and quantitative analysis in various fusion methods and edge preservation using contourlet are elaborated[2,3]. This transform method with maximum rule for low co-efficient and energy rule for high co-efficient gives better fused image. The combination of PCA and dual tree complex wavelet method improves fusion approach for MR plus CT to refine spectral and spatial information as well as soft tissue details of tumor[4]. The lack of phase information and over shift sensitivity was overcome by weighted fusion using Daubachies complex wavelet transform[5–7]. To make diagnosis much easier and accurate there is a need to select a proper wavelet kernel and fusion rule along with their objective evaluation[8,9]. The limitations of 2-D analysis due to lack of directional sensitivity by Wavelet Transform (WT) can be overcome by using shearlet transform and is also recommended for 3-D analysis[10,11].

Angoth Vivek et.al.[12–14] proposed an efficient wavelet based algorithm to detect the size and location of brain tumour by utilizing the complementary and redundant information from imaging modality. The review of quality metric to validate fused image on the basis of different parameters like SNR, PSNR, mutual information, SSIM, etc. are reported[15–17]. Wavelet based image fusion approach is used to detect the size and shape by evaluation of similarity metric[18]. Identification of stages of cancer, based on different classifiers and feature extraction, is proposed for diagnosis[21]. Authors have proposed Discrete WT with HH band decomposition due to micro-calcification of cancer tissues in breast[22]. A detailed review on cancer diagnosis in various organs is carried out with WT using ultrasound images[23].Use of color graphs for mapping stages of cancer with structural method[24] is proposed for cancer diagnosis. Authors suggested the acoustic source for accurate reconstruction of electrical conductivity and compared different image reconstruction algorithms[25]. Prostate cancer diagnosis by texture analysis is carried out on biopsy sample using computer aided diagnosis for feature extraction, validation and classification[26]. Image fusion of multi-modal images is acquired from PET-Ultrasound for detection of prostate cancer[27]. Computer aided detection for breast cancer by pattern classifiers using wavelet neural network is proposed[28]. The results obtained in[29] correlate respiratory motion with functioning of abdomen or chest using external biomarkers obtained by MRI investigation. The authorsin[30] demonstrated use of ultra-wideband microwave system for breast cancer detection using hemi-spiral antenna array. Early stage cancer detection and segmentation of breast cancer is carried out by combining wavelet and genetic algorithm[31].

Author[32] suggested selection of abnormal portion infected by cancer considering group genes from micro array data. Feature detection of colorectal cancer using one dimensional continuous WT and genetic algorithm for biomarker detection is proposed[33]. The experimental results obtained in[34], characterize mitotic and non-mitotic cells using dual tree continuous WT. Cancer therapy with magnetic fluid RF hyperthermia and COMSOL simulation of liver and breast tissues are carried out in[35–37]. The deep portion of abdomen can be removed by thermotherapy with magnetically excited metallic stents instead of surgery[38,39]. The electric filed strength distribution is determined for brain tumor is reported in[40]. Magnetic materials can be selected to destroy bone cancerous tissue[41].

The rest of paper is divided into two sections, wiz, diagnosis and treatment. In the first section diagnosis is explained with the help of fusion technique which includes WT on PET/CT images. Using image processing algorithm abdominal cancer tumour size in different stages has been determined. In the second section of treatment, various methods such as chemotherapy, radiotherapy, surgery are proposed to be compared with RF module. Implementation of RF module using COMSOL-Multiphysics is explained. The focused derivation after its implementation resulted in the RF heat required for the treatment. Finally detailed graphs of variation of temperature, electrical field distribution, degree of tissue injured at various time instant versus cancer region are shown. The next section concludes the work. After the conclusion compliance with ethical standards is mentioned for your reference.

2. Diagnosis of Cancer Tumour

Abdominal cancer analysis is needed for detection of tumour cells which affects organs producing hormones, for example gastric juices, renal cells and also the inner lining that covers abdominal region. The growth of cancer tissues can be observed in different stages which are as T_1, T_2, T_3 and T_4 which means primary stage i.e. tumour started to grow, grown into the layer of muscles, outer lining and spread up of tumour cell affecting other body parts, respectively.

2.1 Wavelet Based Image Fusion

Image fusion technique not only combines but also enhances region of abnormality, as seen from a set of multimodal images. Output of these systems, result in a single image of high quality. There are various methods for extraction of features from biomedical images such as Fast Fourier Transform (FFT), Discrete Fourier Transform (DFT), Principal Component Analysis (PCA), WT, etc. But WT provides better time-frequency resolution where as FFT gives only frequency resolution. Equation (1), defines the mother wavelet governing the entire WT kernels.

$$W\,f(u,s) = (f, \psi_{u,s}) = \int_{-\infty}^{+\infty} f(t)\frac{1}{\sqrt{s}}\psi^{*}\left(\frac{t-u}{s}\right)dt \quad (1)$$

Depending on the nature of mother wavelet, we have various kernels functions. It provides multi-resolution analysis for signal of any dimension. Particularly for variable separable kernel, 2-D image transform can be simply realized as 2-fold WT of columns followed by rows. In order to preserve the time and frequency, details of the images that are to be fused, wavelet fusion algorithm can be preferred.

2.2 Image Fusion Architecture

The proposed fusion architecture is shown in Figure 1 which consists of registration, analysis, fusion process and synthesis. In the pre-processing part, the registration takes place on real PET/CT multi-modal images. Apply 2-D Discrete WT to these registered images, which decompose into four sub-bands as LL, LH, HL and HH. In the fusion process, fusion operator selects a proper fusion rule (Min, Average and Max rule) to merge individual sub-bands of input images. The synthesis process is carried out by taking inverse WT to produce resultant fused image shown in Figure 2.

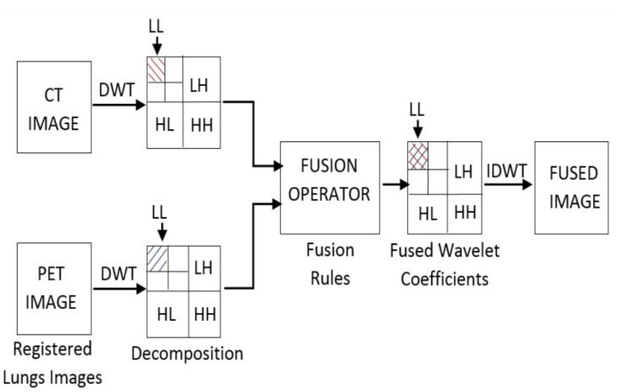

Figure 1. Architecture of proposed image fusion method.

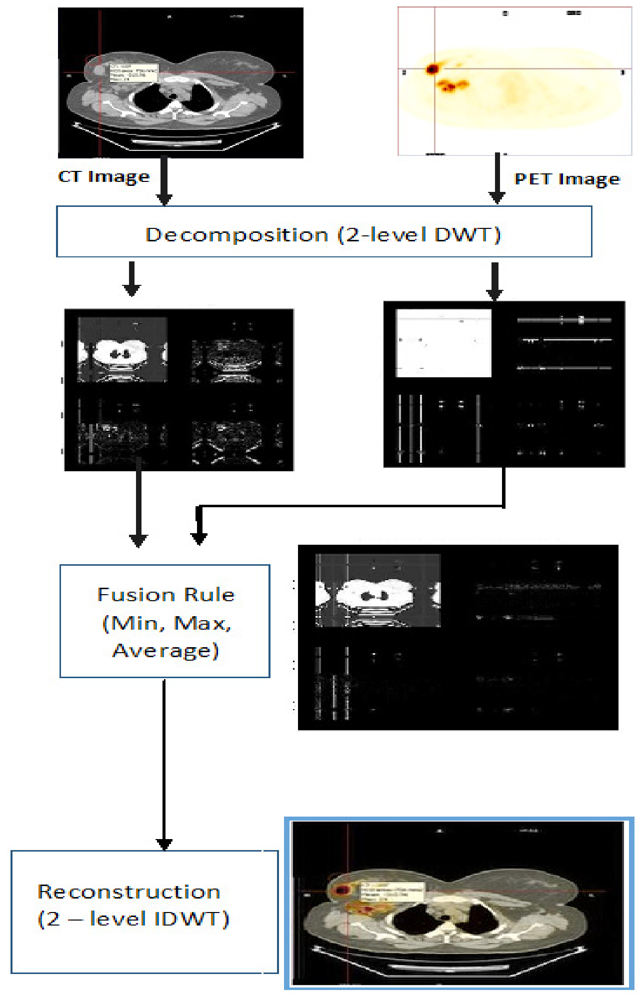

Figure 2. Flow-diagram of wavelet based image fusion.

2.3 Diagnosis Results and Discussions

The quantitative evaluation of this research work using various stages of abdomen cancer has been shown in Table 1, and the performance comparison of the proposed method is accomplished with WT in terms of some non-referential and with reference image quality measures such as Entropy (EN), Average Gradient (AVG_G), Edge Intensity (EI) and Standard Deviation (SD) shown in Figure 3. The superiority as well as robustness of the proposed image fusion technique is evidently justified from the fused image quality of different stages of cancer tumor as shown in Figure 4, Figure 5and Figure 6 respectively. From the image quality assessment tables, it is clear that the proposed fusion technique outperforms stage I, II, III abdomen cancer stages in terms of different quantitative with and without reference parameters as EN, Cross Entropy (CE), AVG_G, EI, SD, Fusion Similarity Metrics (FSM), Spatial Frequency (SF) and Fusion Mutual Information (FMI).

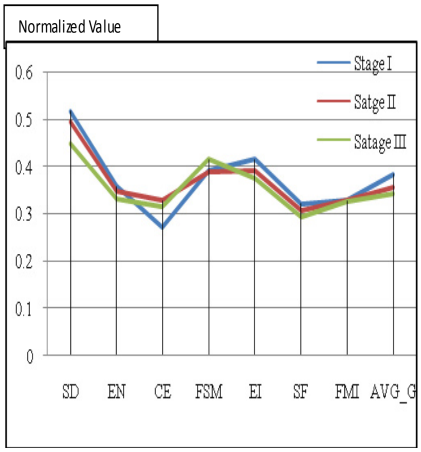

Figure 3. Graphical view of different cancer stages.

Figure 4. Stage I (T1) cancer.

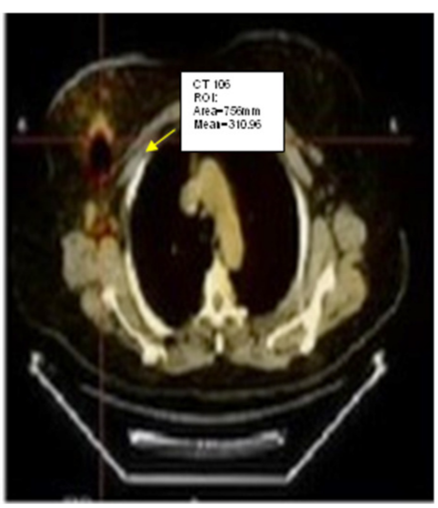

Figure 5. Stage II (T_3) cancer.

Figure 6. Stage III (T_4) cancer.

The calculation of actual size of cancer tumor from PET/CT fused image is given in equation (2)

$$1mm = \frac{N \times K}{dpi} \tag{2}$$

Where, N is number of pixels, *dpi* is 'dots per inch', factor K=25.4 unit is the constant multiplier for this equation. The value of *dpi* is 96 which are measured from image properties. Therefore, we can calculate from equation (2) one pixel=0.26mm approximately. From equation; the actual size of stage- I tumor is 5.55mm ×3.96mm shown in Figure7. Similarly the size of tumor stage II 6.35mm ×8.47mm Figure 8 and Stage III 4.76mm ×5.29mm and 11.64mm ×6.08mm Figure 9 are calculated

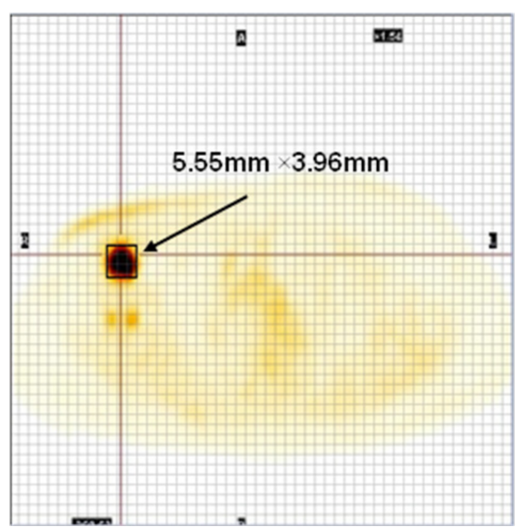

Figure 7. Tumour size of stage I cancer: 5.55mm x 3.96mm.

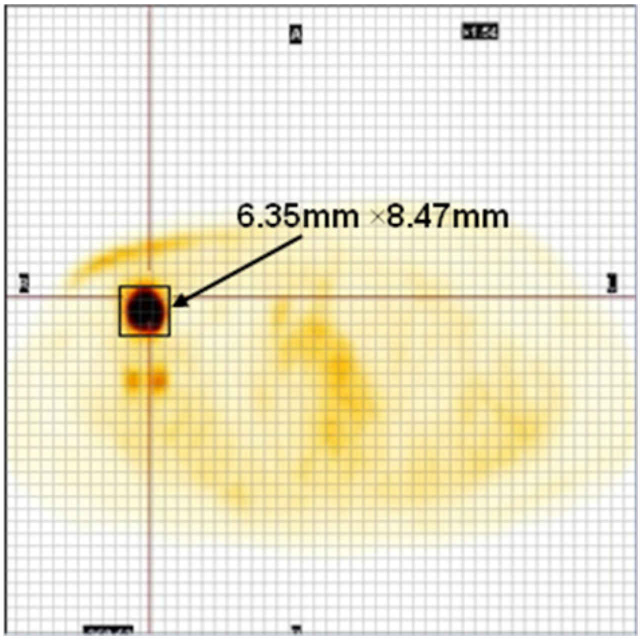

Figure 8. Tumour size of stage II cancer: 6.35mm ×8.47mm.

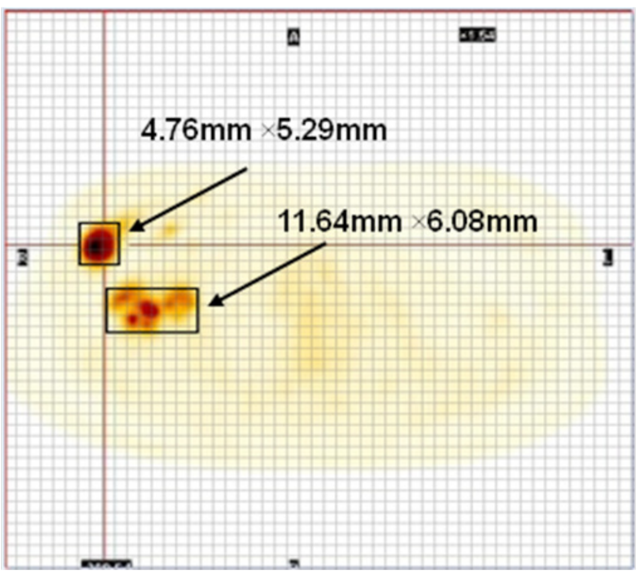

Figure 9. Tumour size of stage III cancer: 4.76mm ×5.29mm and 11.64mm ×6.08mm.

3. Cancer Treatment Using COMSOL RF Module

The important issue in the cancer treatment is the influence area of human body by the RF energy to avoid unwanted radiation or heating effects on healthy human tissue[19]. The size of tissue accurately measure using wavelet image fusion techniques. In this section, we expose one method for removing cancerous tumors of size 6.2mm × 8.4mm, from healthy tissue which is to heat the malignant tissue to a critical temperature that kills the cancer cells. The COMSOL provides 2D/3D flat-form for Electromagnetic heat engineering problem. Its multi Physics capabilities can solve Hyperthermic Oncology and it models the electromagnetic field coupled to the bio-heat equation (3).

The modeling issues and techniques are generally applicable to any problem involving electromagnetic heating. The localized heating of cancer tissue in combination with chemotherapy and radio therapy is often used by oncology department. Sometimes, cancer tissue is inside the deep-region of human body. To operate this tissue without affecting the surrounding tissue is a crucial task. The major challenge here is selective heating, spatial distribution of heat (i.e. space distribution of heat) and placement of sensor for RF heating. The small tiny antenna is used for such an operation. The antenna size depends upon the operating frequency. The quarter wavelength antenna length is used.

The model here is designed to get the temperature distribution and Specific Absorption Rate (SAR)[20]. Specific absorption rate is calculated using equation [3]

$$SAR = \frac{\text{Absorbed heat Power}}{\text{Tissue density}} \tag{3}$$

The temperature distribution is calculated using time dependent bio-heat equation (1). The acceleration of charges is dependent upon the frequency of operation.

Table 1. Objective evaluation of various stages of abdomen cancer

Cancer Stages	SD	EN	CE	FSM	EI	SF	FMI	AVG_G
Stage I	0.516999	0.358389	0.272011	0.390624	0.415408	0.320852	0.327888	0.384203
Stage II	0.495129	0.347432	0.327603	0.389658	0.3902	0.306917	0.327484	0.356941
Stage III	0.448301	0.331756	0.314544	0.415117	0.375245	0.293694	0.32499	0.343706

Higher the rate of acceleration gives more current flow in the terminating device. The electrical field distribution can be adjusted by using the electric current interface which couple to the bio-heat equation. The simplified model of heat and electricity is presented in this paper.

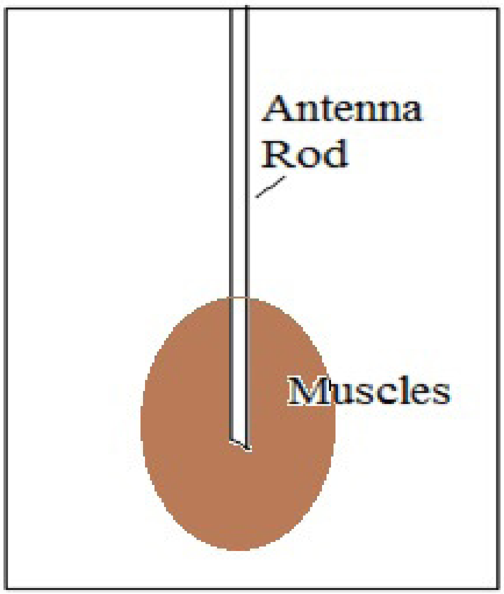

Figure 10. The schematic of antenna has one wavelength dimension.

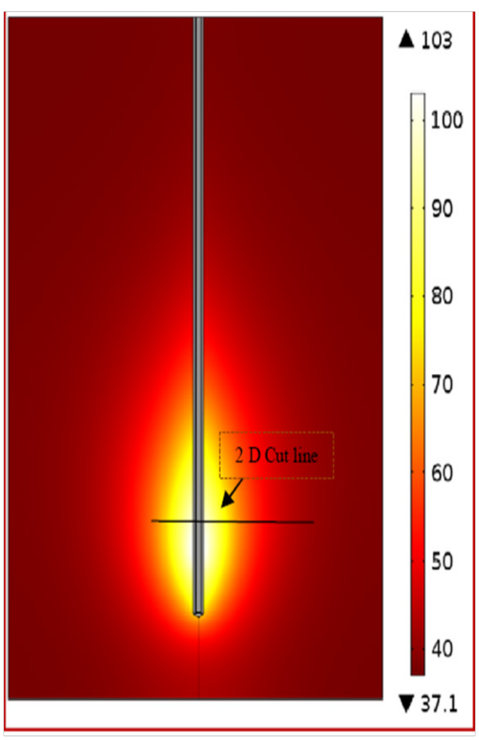

Figure 11. Visualization of the region that has reached 50 °C at 8 minutes.

The tumour tissue can be burnt at an about 45°C to 50°C. Thus, it is necessary to create the localized heating up to 45°C to 50°C. The inserted electrode is electrically insulated. The antenna has single monopole type of rods for radiation. The schematic antenna is shown in Figure 10. The electric current through the connecting rod has stronger resistive heating loss at tumour.

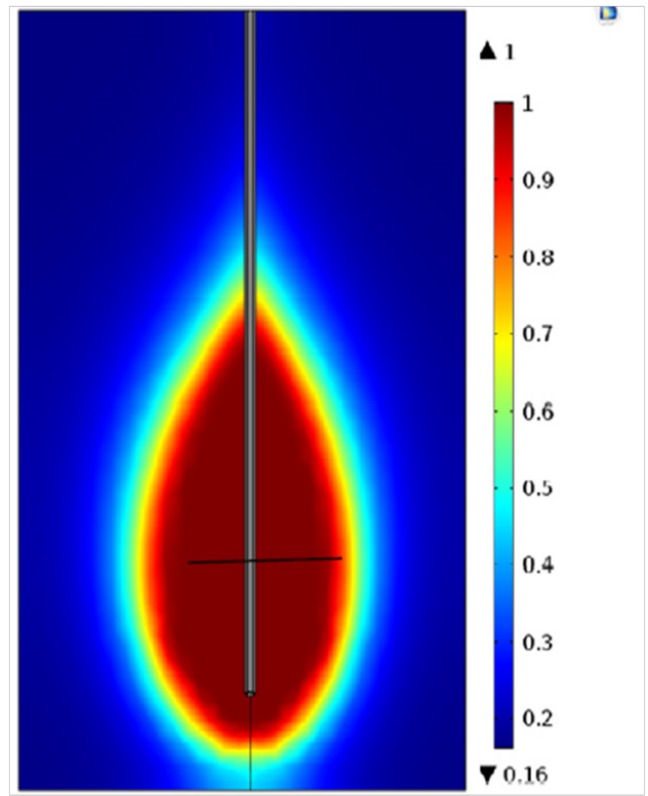

Figure 12. Fraction of necrotic tissue.

The model locates the probe along the cylinder's center line with its electrodes span the region where the tumour is located. The geometry also includes a large blood vessel. The normal temperature at initial condition is 37°C which is called heat sources from metabolism (Q_{met}). The planner view temperature variation in the muscle region is shown in Figure 11. The damage of cancer tissue is shown in Figure 12.

The bio-heat equation governs heat transfer in the tissue-

$$\delta_{ts}\rho C\frac{\partial T}{\partial t} + \nabla\cdot(-k\nabla T) = \rho_b C_b \omega_b (T_b - T) + Q_{met+ext} \quad (4)$$

Where, δ_{ts}- Time-scaling coefficient;

ρ - Tissue density (kg/m3);

C -Tissue's specific heat (J/(kg·K));
k - Thermal conductivity (W/(m·K));
ρ_b- Blood's density (kg/m3);
C_b- Blood's specific heat (J/(kg·K));
ω_b- Perfusion rate (1/s);
T_b- Arterial blood temperature (K);

Heat sources are from metabolism and external heating (W/m3).

$$E = e_r \frac{C}{r} e e^{j(wt-kz)} \tag{5}$$

$$H = e_\varphi \frac{C}{Z} e e^{j(wt-kz)} \tag{6}$$

$$Pav = \int_{r_{inner}}^{r_{outer}} Re\left(\frac{1}{2} E \times H^*\right) 2\pi r dr = e_z \pi \frac{C^2}{Z} \ln\left(\frac{r_{outer}}{r_{inner}}\right) \tag{7}$$

Where, $K = \frac{2\pi}{\lambda}$

$$\nabla \times \left(\left(\varepsilon r - \frac{j\sigma}{\omega \varepsilon_0}\right)^{-1} \nabla \times H_\varphi\right) - \mu_r k^2 H_\varphi = 0 \tag{8}$$

Where, $n \times E = 0$

$$n \times \sqrt{\varepsilon} E - \sqrt{\mu} H_\varphi = -2\sqrt{\mu} H_{\varphi 0} \tag{9}$$

$$H_{\varphi 0} = \frac{\sqrt{\dfrac{P_{av} Z}{\pi r \ln\left(\frac{r_{outer}}{r_{inner}}\right)}}}{r} \tag{10}$$

$$Q_{ext} = \frac{1}{2} Re[(\sigma - jw\varepsilon) E \cdot E^*] \tag{11}$$

Where, $n \cdot \nabla T = 0$

$$\frac{d\alpha}{dt} = A\ exp\left(-\frac{dE}{RT}\right) \tag{12}$$

Thus,

$$\theta_d = 1 - exp(-\alpha) \tag{13}$$

In this model, the bio-heat equation also models heat transfer in various parts of the probe with the appropriate values for the specific heat, C (J/ (kgK)), and thermal conductivity, k(W/(mK)). The degree of tissue injured (α), can be calculated from the equation (13).

The process of shrinking the tissue is one of the important steps in cancer treatment. This can be achieved by electromagnetic heat generation process. The RF energy is deposited into the cancer tissue using antenna shown in Figure12. The RF to heat conversion is formulated using following equation.

$$\rho Cp \frac{\partial T}{\partial t} + \rho Cp U . \nabla T = \nabla . (k \nabla T) + Q \tag{14}$$

The space and time relation for the electromagnetic wave is derived from the Faraday's law of induction given in equation (15).

$$\nabla \times E = -\frac{\partial B}{\partial t} \tag{15}$$

The relation between magnetic flux density and intensity is given by equation (16).

$$B = \mu H \tag{16}$$

Thus,

$$\nabla \times E = -\frac{\partial \mu H}{\partial t} \tag{17}$$

$$\nabla \times E = -\mu \frac{\partial H}{\partial t} \tag{18}$$

Taking the curl on both side-

$$\nabla \times \nabla \times E = \nabla \times \left(-\mu \frac{\partial H}{\partial t}\right) \tag{19}$$

$$\nabla^2 E = -\mu \frac{\partial(\nabla \times H)}{\partial t} \tag{20}$$

Where, ∇ is the space variation also called spatial derivative denoted by-

$$\nabla = \frac{\partial}{\partial x} + \frac{\partial}{\partial y} + \frac{\partial}{\partial z} \tag{21}$$

$$\frac{\partial^2 E_x}{\partial x^2} + \frac{\partial^2 E_y}{\partial y^2} + \frac{\partial^2 E_z}{\partial z^2} = -\mu\varepsilon \left(\frac{\partial^2 E_x}{\partial t^2} + \frac{\partial^2 E_y}{\partial t^2} + \frac{\partial^2 E_z}{\partial t^2}\right) \tag{22}$$

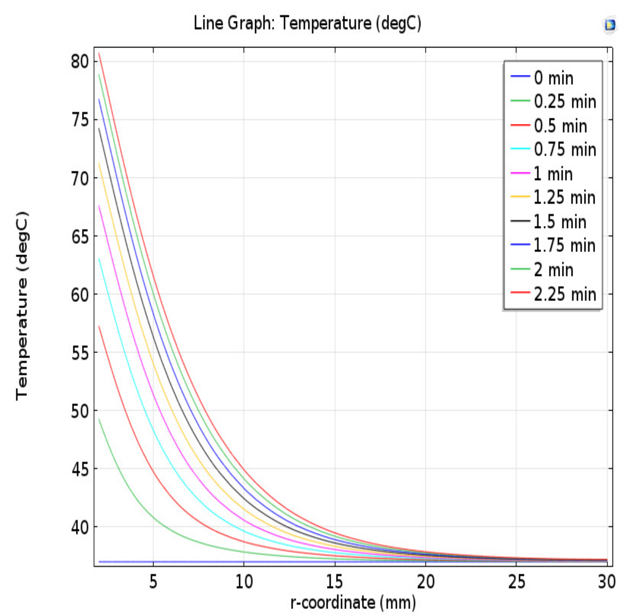

Figure 13. Variation of tumor effective space (mm) versus temperature (degC).

The space versus time is an important relation for the further analysis such as temperature, E-field variation versus space. Figure 13 shows the line graph along r-coordinate versus temperature for RF effective area of cover. This plot shows the maximum area covered up to 30 mm which is the normal size of human abdomen cancer tumor. The exceeded size of tumour can be tested under different size of antenna. The antenna used in this RF heating is 5 mm in length. We define the r-coordinate as a 2D cut line on the tumor cell shown in Figure11. This cut line on 2D is defined from 2.5 mm to 30 mm along the x-axis named as r-coordinate. Thus, plots shown in Figure 13, Figure 14, and Figure 15 varied from 2.5mm to 30 mm.

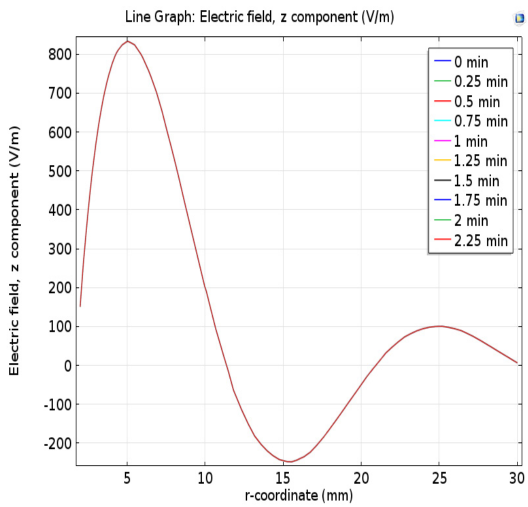

Figure 14. Z-component of electric field intensity (V/m) versus space (mm).

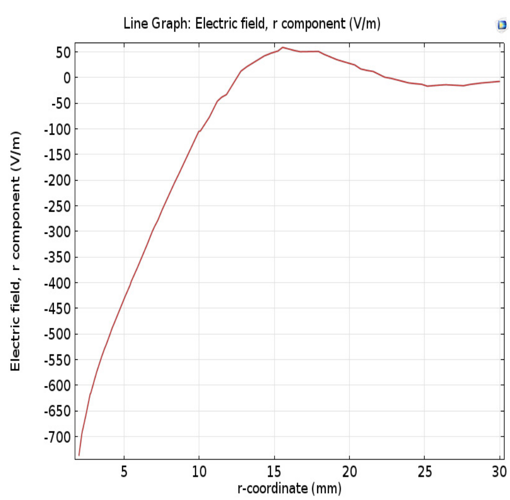

Figure 15. r-component of electric field intensity (V/m) versus space (mm).

The variation of z-component and r-component of electric field intensity (V/m) versus space (mm) is shown in Figure 14 and Figure 15 respectively. The temperature (degC) variation at various time steps is shown in Figure 16. The variation of temperature versus z-component of electric field intensity is plotted to understand the nonlinear relationship for treatment. This nonlinear plot is shown in Figure 17. The degree of tissue injury versus temperature and space are shown in Figure18 and Figure 19 respectively.

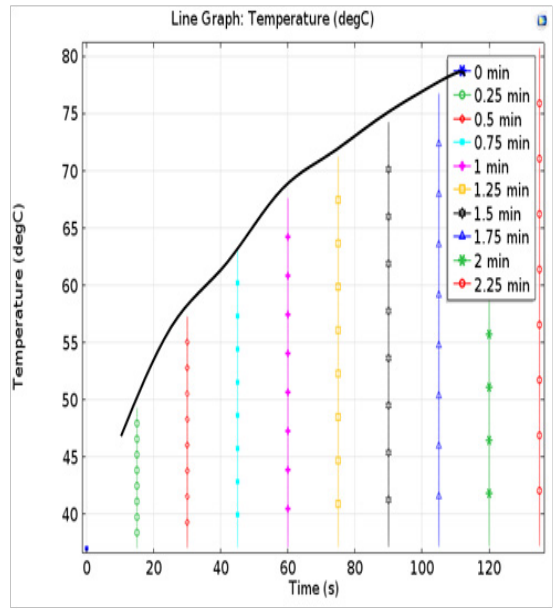

Figure 16. The temperature (degC) variation at various time steps (sec.).

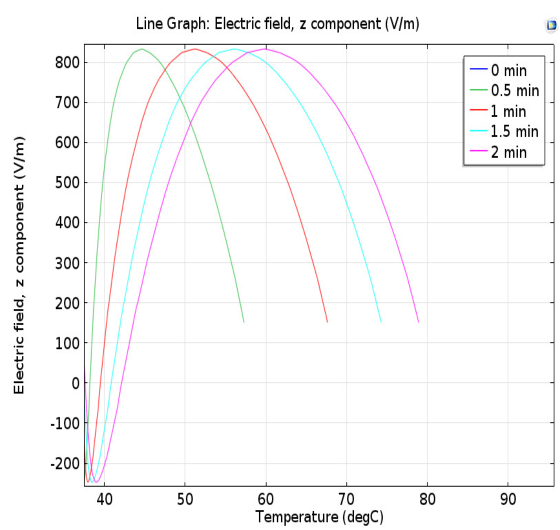

Figure 17. Temperature versus z-component of electric field intensity (V/m).

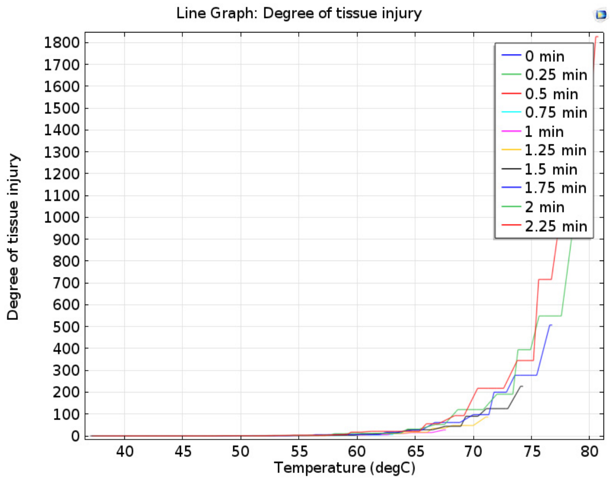

Figure 18. Degree of tissue injury versus temperature (degC).

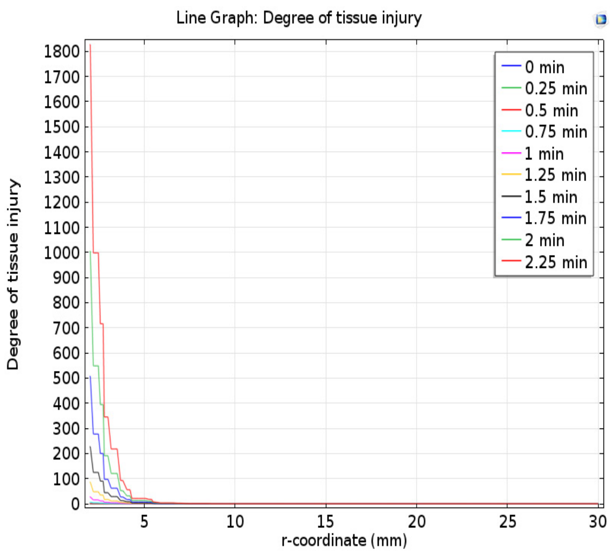

Figure 19. Degree of tissue injury versus space (mm).

4. Conclusion

The value aided information and visualization in image fusion, helps doctor in rapid and efficient cancer detection which reduces time as well as efforts. The manuscript presents comparison between different stages of abdomen cancer tumor with their growth. The wavelet function and fusion rules together are optimized using various qualitative parameters such as CE, FMI, EI, fusion quality index, etc. The COMSOL-Multiphysics modeling of cancer tissue treatment is achieved effectively. Hence results shows the significant contribution towards the treatment of cancer tissue size varies from 5.55 mm to 11.64 mm at various stages. The planner view of temperature variation and degree of damage of cancer tissue are presented with color legend which can help medical practitioners. Finally it is concluded that the 45^{0}C to 50^{0}C temperature is sufficient to burn the cancer cells (5.5 mm to 11.64 mm size) in 0.25 min to 0.5 min.

5. Compliance with Ethical Standards

All procedures performed in this study involve human participants who are in accordance with the ethical standards of the Padmashree Dr. D.Y. Patil Medical College & Hospital and Research Centre Institutional Ethics Committee (Ref. No. PDYPMC/Ethics/Sept-02/2015) and its later amendments are comparable with ethical standards. We have complied with the ICH-GCP ethical guidelines regarding research with human participants and in the conduct of the research presented in this manuscript.

6. References

1. Lu Y, Zhao J, Wang G. Edge-guided dual-modality image reconstruction. Institute of Electrical and Electronics Engineers (IEEE) Access. 2014 Nov 20; 2:1359–63.
2. Haribabu M, Bindu CHH, Prasad KS. Image fusion with biorthogonal wavelet transform based on maximum selection and region energy. In the Proceedings of the Institute of Electrical and Electronics Engineers (IEEE) International Conference Computer Communication and Informatics, Coimbatore, India; 2014 Jan 3–5. p. 1–6.
3. Upla PK, Joshi VM, Gajjar PP. An edge preserving multiresolution fusion: use of contourlet transform and MRF prior. Institute of Electrical and Electronics Engineers (IEEE) Transactions on Geoscience and Remote Sensing. 2015 Jun; 53(6):3210–20. Crossref.
4. Himanshi, Bhateja V, Krishn A, Sahu A. An improved medical image fusion approach using PCA and complex wavelets. In the Proceedings of the Institute of Electrical and Electronics Engineers (IEEE) International Conference Medical Imaging, m-Health and Emerging Communication Systems, Greater Noida, India; 2014 Nov 7–8. p. 442–7.
5. Singh R, Khare A. Multimodal medical image fusion using Daubechies complex wavelet transforms. In the Proceedings of the Institute of Electrical and Electronics Engineers (IEEE) Conference on Information and Communication Technologies (ICT), Thuckalay, Tamil Nadu, India; 2013 Apr 11–12. p. 869–73.

6. Gupta VR, Agarwal VK, Tade SL. Comparison of medical image fusion algorithm for preserving the edge information based on improved wavelet coefficient contrast. International Journal of Emerging Technology and Advanced Engineering. 2012 May; 2(5):328–33.
7. Sweeti, Kaur M, Singh B, Anand S. A novel method for medical image fusion and comparative analysis. International Journal of Current Engineering and Technology. 2013 Dec; 3(5):1708–15.
8. Jagalingam P, Hegde AV. A review of quality metrics for fused image. Aquatic Procedia, Elsevier, ScienceDirect. 2015; 4:133–42. Crossref.
9. Parmar K, Kher R. A comparative analysis of multimodality medical image fusion methods. In the Proceedings of the Institute of Electrical and Electronics Engineers (IEEE) 6th Asia Modelling Symposium (AMS), Bali, Indonesia; 2012 May 29–31. p. 93–7. Crossref.
10. Wang L, Li B, Tian L. Multimodal medical volumetric data fusion using 3-D discrete shearlet transform and global-to-local rule. Institute of Electrical and Electronics Engineers (IEEE) Transactions on Biomedical Engineering. 2014 Jan; 61(1):197–206. Crossref.
11. Fuster BM, Esteban O, Thielemans K, Setoain X, Santos A, Ros D, Pavia J. Including anatomical and functional information in MC simulation of PET and SPECT brain studies brain-VISET: a voxel-based iterative method. Institute of Electrical and Electronics Engineers (IEEE) Transactions on Medical Imaging. 2014 Oct; 33(10):1931–8. Crossref.
12. Angoth V, Dwith CYN, Singh A. A novel wavelet based image fusion for brain tumor detection. International Journal of Computer Vision and Signal Processing. 2013 Feb 18; 2(1):1–7.
13. Krause BJ, Souvatzoglou M, Tuncel M, Herrmann K, Buck AK, Praus C, Schuster T, Geinitz H, Treiber U, Schwaiger M. The detection rate of [11C] choline-PET/CT depends on the serum PSA-value in patients with biochemical recurrence of prostate cancer. European Journal of Nuclear Medicine and Molecular Imaging. 2008 Jan; 35(1):18–23. Crossref.
14. Wang X, Ballangan C, Cui H, Fulham M, Eberl S, Yin Y, Feng D. Lung tumor delineation based on novel tumor-background likelihood models in PET-CT images. Institute of Electrical and Electronics Engineers (IEEE) Transactions on Nuclear Science. 2014 Feb; 61(1):218–24. Crossref.
15. Wang Z, Bovik AC. A universal image quality index. Institute of Electrical and Electronics Engineers (IEEE) Signal Processing Letters. 2002 Mar; 9(3):81–4. Crossref.
16. Saini V, Gulati T. A comparative study on image enhancement using image fusion. International Journal of Advanced Research in Computer Science and Software Engineering. 2012 Oct; 2(10):141–5.
17. Bedi SS, Agarwal J, Agarwal P. Image fusion techniques and quality assessment parameters for clinical diagnosis: a review. International Journal of Advanced Research in Computer and Communication Engineering. 2013 Feb; 2(2):1153–7.
18. Cvejic N, Seppanen T, Godsill SJ. A nonreference image fusion metric based on the regional importance measure. Institute of Electrical and Electronics Engineers (IEEE) Journal of Selected Topics in Signal Processing. 2009 Sep; 3(2):212–21. Crossref.
19. Tungjitkusolmun S, Staelin ST, Haemmerich D, Tsai JZ, Cao H, Webster JG, Lee FT, Mahvi DM, Vorperian VR. Three-dimensional finite element analyses for radio-frequency hepatic tumor ablation. Institute of Electrical and Electronics Engineers (IEEE) Transactions on Biomedical Engineering. 2002 Jan; 49(1):3–9. Crossref.
20. Saito K, Taniguchi T, Yoshimura H, Ito K. Estimation of SAR distribution of a tip-split array applicator for microwave coagulation therapy using the finite element method. The Institute of Electronics, Information and Communication Engineers (IEICE) Transactions on Electronics. 2001 Jul 1; E84–C(7):948–54.
21. Ergin S, Kilinc O. A new feature extraction framework based on wavelets for breast cancer diagnosis. Journal of Computers in Biology and Medicine. 2014 Aug; 51:171–82.
22. Lahmir S. A wavelet based processing approach for microcalcifications detection in mammograms. Journal of Advances in Information Technology. 2012 Aug; 3(3):162–7. Crossref.
23. Sudarshan KV, Mookiah MR, Acharya UR, Chandran V, Molinari F, Fujita H, Ng KH. Application of wavelet techniques for cancer diagnosis using ultrasound images: a review. Journal of Computers in Biology and Medicine. 2015 Dec; 69:98–113.
24. Altunbay D, Cigir C, Sokmensuer C, Demir CG. Color graphs for automated cancer diagnosis and grading. Institute of Electrical and Electronics Engineers (IEEE) Transactions on Biomedical Engineering. 2010 Mar; 57(3):665–74. Crossref.
25. Xia R, Li X, He B. Comparison study of three different image reconstruction algorithms for MAT-MI. Institute of Electrical and Electronics Engineers (IEEE) Transactions on Biomedical Engineering. 2010 Mar; 57(3):708–13. Crossref.
26. Lopez CM, Agaian S, Hoyos AV, Thompson I. Computer-aided prostate cancer diagnosis from digitized histopathology: a review on texture-based systems. Institute of Electrical and Electronics Engineers (IEEE) Transactions on Biomedical Engineering. 2014 Jul 17; 8:98–113. Crossref.
27. Huber SJ, Peng Q, Moses WW, Reutter WB, Pouliot J, Hsu IC. Development of a PET-transrectal ultrasound pros-

tate imaging system. Institute of Electrical and Electronics Engineers (IEEE) Transactions on Nuclear Science. 2011 Jun; 58(3):674–81. Crossref.

28. Dheeba J, Singh NA, Selvi ST. Computer-aided detection of breast cancer on mammograms: a swarm intelligence optimized wavelet neural network approach. Journal of Biomedical Informatics, Elsevier, ScienceDirect. 2014 Jun; 49:45–52. Crossref.
29. Dasari P, Johnson K, Dey J, Lindsay C, Shazeeb MS, Mukherjee JM, Zheng S, King AM. MRI investigation of the linkage between respiratory motion of the heart and markers on patient's abdomen and chest: implications for respiratory amplitude binning list-mode PET and SPECT studies. Institute of Electrical and Electronics Engineers (IEEE) Transactions on Nuclear Science. 2014 Feb; 61(1):192–201. Crossref.
30. Klemm M, Craddock IJ, Leendertz JA, Preece A, Benjamin R. Radar-based breast cancer detection using a hemispherical antenna array—experimental results. Institute of Electrical and Electronics Engineers (IEEE) Transactions on Antennas and Propagation. 2009 Jun; 57(6):1692–704. Crossref.
31. Pereiraa DC, Ramosb RP, Nascimentoc MZD. Segmentation and detection of breast cancer in mammograms combining wavelet analysis and genetic algorithm. Computer Methods and Programs in Biomedicine, Elsevier, ScienceDirect. 2014 Apr; 114(1):88–101.
32. Sun X, Liu Y, Wei D, Xu M, Chen H, Han J. Selection of interdependent genes via dynamic relevance analysis for cancer diagnosis. Journal of Biomedical Informatics, Elsevier, ScienceDirect. 2013 Apr; 46(2):252–8. Crossref.
33. Liu Y, Aickelin U, Feyereisl J, Durrant LG. Wavelet feature extraction and genetic algorithm for biomarker detection in colorectal cancer data. Knowledge-Based Systems, Elsevier, ScienceDirect. 2013 Jan; 37:502–14. Crossref.
34. Wan T, Liu W, Chen J, Qin Z. Wavelet-Based Statistical Features For Distinguishing Mitotic And Non-Mitotic Cells In Breast Cancer Histopathology. In the Proceedings of the Institute of Electrical and Electronics Engineers (IEEE) International Conference on Image Processing (ICIP), Paris, France. 2014 Oct 27–30. p. 2290–4.
35. Pavel M, Stancu A. Study of the optimum injection sites for a multiple metastases region in cancer therapy by using MFH. Institute of Electrical and Electronics Engineers (IEEE) Transactions on Magnetics. 2009 Oct; 45(10):4825–8. Crossref.
36. Habault D, Dery A, Leng J, Lecommandoux S, Le Meins JF, Sandre O. Droplet microfluidics to prepare magnetic polymer vesicles and to confine the heat in magnetic hyperthermia. Institute of Electrical and Electronics Engineers (IEEE) Transactions on Magnetics. 2013 Jan; 49(1):182–90. Crossref.
37. Wang SY, Huang S, Andra D, Tasciuc B. Potential sources of errors in measuring and evaluating the specific loss power of magnetic nanoparticles in an alternating magnetic field. Institute of Electrical and Electronics Engineers (IEEE) Transactions on Magnetics. 2013 Jan; 49(1):255–62.
38. Shoji H, Ozu Y, Sato F, Matsuki H, Satomi S, Nihei Y, Kurokawa Y, Sato T. Thermotherapy with metallic stent heated by external magnetic excitation. Institute of Electrical and Electronics Engineers (IEEE) Transactions on Magnetics. 2005 Oct; 41(10):4167–9. Crossref.
39. Tai CC, Chen CC, Kuo CC, Lin FW, Chang CJ, Chen YH, Wang WC. Deep-Magnetic –Field generator using flexible laminated copper for thermotherapy applications. Institute of Electrical and Electronics Engineers (IEEE) Transactions on Magnetics. 2014 Nov; 50(11):9100504–7. Crossref.
40. Lee EG, Duffy W, Hadimani RL, Waris M, Siddiqui W, Isalam F, Rajamani M, Nathan R, Jiles DC. Investigational effect of brain-scalp distance on the efficacy of transcranial magnetic stimulation treatment in depression. Institute of Electrical and Electronics Engineers (IEEE) Transactions on Magnetics. 2016 Jul; 52(7):5000804–7.
41. Shankhwar N, Singh RK, Kothiyal GP, Perumal A, Sriniwasan A. Evaluation of magnetic properties of CaO-P2O5-Na2O-Fe2O3-SiO2 glass upon heat treatment. Institute of Electrical and Electronics Engineers (IEEE) Transactions on Magnetics. 2015; 50(1):4003504–7.